Characterization of dynamic morphological changes of tin anode electrode during (de)lithiation processes using in operando synchrotron transmission X-ray microscopy

Tianyi Li[1], Xinwei Zhou[1], Yi Cui[1], Cheolwoong Lim[1], Huixiao Kang[1], Bo Yan[2], Jiajun Wang[3], Jun Wang[3], Yongzhu Fu[4], and Likun Zhu[1*]

[1]Department of Mechanical and Energy Engineering, Indiana University Purdue University Indianapolis, Indianapolis, IN 46202

[2]School of Materials Science and Engineering, Shanghai Jiao Tong University, Shanghai, 200030, China

[3]Photon Sciences Directorate, Brookhaven National Laboratory, Building 744 Ring Road, Upton, NY 11973

[4]College of Chemistry and Molecular Engineering, Zhengzhou University, Zhengzhou 450001, China

[*]Corresponding Author:

Likun Zhu

Department of Mechanical and Energy Engineering

Indiana University Purdue University Indianapolis

723 W. Michigan Street, Room SL 260 L

Indianapolis, IN 46202

Phone: 1-317-274-4887

Fax: 1-317-274-9744

Email: likzhu@iupui.edu

_____

Abstract:

The morphological evolution of tin particles with different sizes during the first lithiation and delithiation processes has been visualized by an in operando synchrotron transmission X-ray microscope (TXM). The in operando lithium ion battery cell was operated at constant current condition during TXM imaging. Two-dimensional projection images with 40 nm resolution showing morphological evolution were obtained and analyzed. The analysis of relative area change shows that the morphology of tin particles with different sizes changed simultaneously. This phenomenon is mainly due to a negative feedback mechanism among tin particles in the battery electrode at a constant current operating condition. For irregular-shaped tin particles, the contour analysis shows that the regions with higher curvature started volume expansion first, and then the entire particle expanded almost homogeneously. This study provides insights for understanding the dynamic morphological change and the particle-particle interactions in high capacity lithium ion battery electrodes.

1. Introduction

Advanced lithium ion battery (LIB) technologies have been considered promising in the realization of electric vehicles because they have high energy and power density relative to other cell chemistries [1-4]. During the last decade, many research efforts have been made to develop alloy-type anode materials for LIBs, because of their much higher storage capacity compared to graphite (372 mAh g^{-1}) [5]. Tin (Sn) is one of the alloy-type materials and it has a theoretical capacity of 994 mAh g^{-1} (for the charged $Li_{22}Sn_5$ phase) [6-8]. Sn is also non-toxic, abundant and inexpensive. However, the major challenge in the development of Sn anode is the large volumetric change (about 360%) involved in the reaction scheme, which could result in particle fracture and electrode delamination from the current collector, thereby leading to a rapid loss of specific capacity [6, 9-13]. Particle fracture can be alleviated by nano-structuring the alloy-type anode materials due to the facile strain accommodation and the short diffusion path for electron and lithium transport in the nano-structured electrodes [14-18]. However, nano-structured particles have low tap density and lead to lower energy density anodes, making scale-up difficult [19]. In addition, the surface area of the material increases with decrease in particle size, which leads to a large irreversible capacity loss due to the formation of the solid electrolyte interphase (SEI) [6]. Another approach to withstanding the massive strain in high capacity anode materials is to design composites containing both high capacity anode material and stress-accommodating phase [6]. Although the composite anode material can alleviate the particle fracture, the large volume change still exists and it is a dynamic process during the cycling of a LIB. Therefore, it is essential to understand the dynamic morphological change of Sn electrodes in LIB cycling processes.

To this end, several in situ studies have been conducted to investigate the morphological change of Sn electrodes. For instance, Ebner et al. used X-ray tomography to visualize and quantify the origin and evolution of electrochemical and mechanical degradation of a tin oxide electrode [20]. Sun et al. used in situ synchrotron radiography to investigate the lithiation and delithiation mechanisms of multiple Sn particles in a customized flat radiography cell [21]. Wang et al. studied the microstructural change of a Sn electrode using in situ synchrotron X-ray nano-tomography [22]. Recently, Zhou et al. reported the evolution of the microstructure of a single Sn particle battery using in situ focused ion beam-scanning electron microscopy [12]. These in situ and operando studies have revealed the dynamic morphology and microstructure change of Sn particles. However, the real LIB electrodes are composed of Sn particles with different sizes and shapes, and the electrochemical performance of the whole cell is on the multiple-particle scale. We hypothesize that the interaction between particles and the shape irregularity of the particle could affect the dynamic morphological change of Sn particles. The single particle study and the homogeneous electrode assumption (same particle size and spherical shape) cannot help to test this hypothesis.

Therefore, the objective of this paper is to investigate the morphological evolution of a Sn electrode made of particles with different sizes and shapes. We want to answer the following two questions in this paper. (1) Does the morphology of Sn particles with different sizes change simultaneously? (2) Does an irregular-shaped Sn particle have a homogeneous morphology change? In this work, we studied morphological evolution of Sn electrodes via in operando synchrotron transmission X-ray microscopy (TXM) at the Beamline 8-BM-B of Advanced Photon Source (APS) which is operated by the National Synchrotron Light Source-II (NSLS-II)

4

through an NSLS-II transition program. Two-dimensional (2D) projection images of Sn particles in the Sn electrode were obtained and analyzed to study the effect of particle size and shape on the dynamic morphological change during the lithiation and delithiation processes. Ex situ X-ray diffraction (XRD) was implemented to monitor the crystalline change and the XRD results were used to interpret the morphological evolution data.

2. Experimental

2.1 Materials

Sn powder (Sn, 10 μm, 99% trace metals basis, Sigma-Aldrich), super C65 conductive carbon black (Timcal Co., Ltd.), polyvinylidene fluoride binder (PVDF, 12 wt.%, Kureha Battery Materials Japan Co., Ltd.), 1-methyl-2-pyrrolidinone (NMP, anhydrous 99.5%, Sigma-Aldrich), 1M $LiPF_6$ electrolyte in 1:1 volume ratio mixture of ethylene carbonate and dimethyl carbonate solution (BASF Corporation), pyrolytic graphite sheet as current collector (MTI corporation), lithium ribbon (thickness of 0.38mm, 99.9% trace metals basis, Sigma-Aldrich) were purchased from commercial corporations and utilized as received.

2.2 Preparation of Sn electrode

To investigate the morphological and phase change of Sn particles, Sn electrodes for TXM and XRD were fabricated from a 25:45:30 (weight%) mixture of Sn, carbon black, and PVDF. A low percentage of Sn was used to avoid the overlaps of Sn particles during TXM imaging. The mixture was added into NMP solution and mixed homogeneously by a magnetic stir bar in a vial for 20 h. The gel-like slurry was coated onto a thin pyrolytic graphite sheet via a film casting

5

doctor blade (EQ-Se-KTQ-100, MTI, Richmond, CA, USA). Graphite sheet was used as the

current collector to avoid strong X-ray absorption from the current collector during TXM

imaging. The electrode was dried at 100 °C in a vacuum oven for 12 h. As shown in Fig. 1a, Sn

particles were uniformly distributed and the particle size was between 1 to 10 µm. The thickness

of the Sn electrode is about 9 µm as shown in Fig. 1b. Circular discs with 1.11 cm in diameter

were cut out of the Sn electrode film for cell assembly. The mass loading of Sn on the graphite

current collector is approximately 0.3 mg cm^{-2}. All the cut Sn electrodes were stored in an argon-

filled glove box.
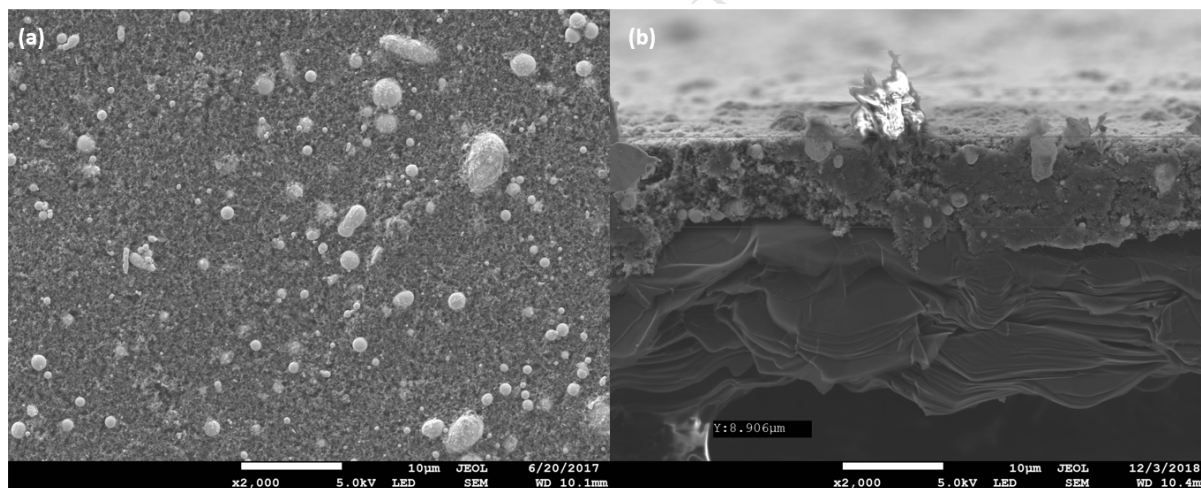
Fig. 1. SEM images for (a) the top surface and (b) the cross-section a Sn electrode. The Sn

electrode was fabricated from a 25:45:30 (weight%) mixture of Sn, carbon black, and PVDF.

The scale bar is 10 µm.

2.3 Coin cell assembly and electrochemical evaluation

6

CR2032 coin cells were modified and used in this study. Briefly, 2 mm diameter holes were punched at the center of the anode and cathode cases. 30 µm thick Kapton tape was used to seal the hole on both sides of the case. The cells were assembled in an argon-filled glovebox (under $O_2 < 0.1$ ppm, $H_2O < 0.1$ ppm; Unilab 2000, Mbraun, Stratham, NH, USA) as shown in Fig. 2a. First, a Sn electrode was placed on the anode case with the graphite side facing down, followed by adding 15 µL electrolyte. A Celgard 2400 separator was placed on top of the Sn electrode and another 15 µL electrolyte was added on top of the separator. Then a piece of lithium metal (1.27 mm in diameter) was placed on the separator. Finally, a stainless-steel plate (with a 2 mm hole at the center) covered the lithium metal with a spring as the spacer. The cell was crimped and taken out of the glove box for electrochemical evaluation.

The in operando coin cell was galvanostatically cycled from open circuit potential to 0.01 V at 0.1 C during the first lithiation, at 0.05 C for the second lithiation, and from 0.01 to 1.2 V at 0.1 C for delithiation using an Arbin 2000 battery cycler. The second 0.05 C lithiation was implemented because no morphological changes were detected by the TXM at the end of the first 0.1 C lithiation.
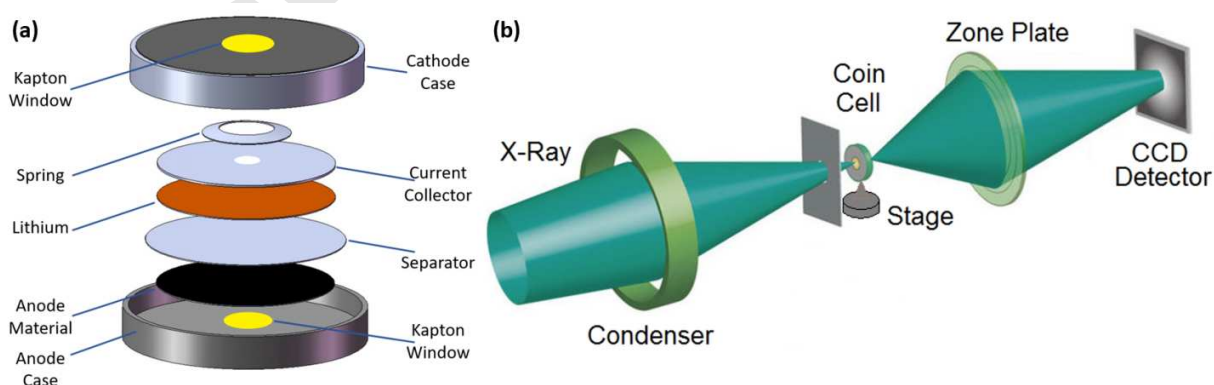
Fig. 2. Schematics of (a) the in operando coin cell assembly and (b) the synchrotron transmission X-ray microscopy setup [22].

2.4 In operando transmission X-ray microscopy

Transmission X-ray microscopy is a non-destructive technology to perform nano-imaging. The synchrotron TXM with a large field of view of 40 µm by 40 µm at 40 nm pixel size was employed in this study. This TXM hosted on beamline 8-BM at APS was operated by NSLS-II through an NSLS-II transition program. The 2D in operando TXM images were consecutively collected to visualize and quantify morphological changes of Sn particles under operating condition. We employed a 10 min time interval for data acquisition. Ten different positions were collected consecutively with an exposure time of 3 s for each capture. During the image collecting process at each position, 10 images were captured and averaged to improve accuracy. The overall image collection took 5 min and we adopted a 5 min gap between each series of acquisition. The schematic of the TXM is shown in Fig. 2b.

2.5 X-ray diffraction

An ex situ XRD measurement was performed on a Bruker D8 Discover XRD Instrument equipped with Cu Kα radiation at the Integrated Nanosystems Development Institute (INDI) with a photon wavelength of 1.5406Å. Each coin cell to be measured was cycled to a specific voltage. Electrodes were obtained by dissembling the coin cells. The cycled electrodes were rinsed with diethyl carbonate solution, dried under vacuum for 30 min, and sealed in Kapton tape. We measured 2θ from 20 ° to 60 ° with an increment of 0.02 ° for the XRD experiment. The

exposure time for each increment was 0.5 s. The XRD data were calibrated using the corundum standard and analyzed via DIFFRAC.EVA software.

2.6 Image processing

Image processing was conducted via a commercial software Avizo®. Motion artifacts were observed in the operando experiment due to the movement of the sample during the measurement, such as volume expansion or shrinking of active materials and tilting of the electrode during the data acquisition. Hence, image filtering was employed as the first step in image analysis. All the grayscale images in this work were subject to non-local means filtering to remove noise and blur due to its high efficiency at noise removal [23], followed by register image algorithm in Avizo®. Image registration is the process to transform different sets of images into one coordinate system based on the gravitational center and contour lines for conducting further analysis.

3. Results and discussion

The voltage profile of a Sn cell is shown in Fig. 3a. The Sn electrode was lithiated twice at different C rates (0.1 C and 0.05 C) in order to achieve full lithiation. Fig. 3b shows a series of TXM images at one of the ten positions during the first cycle. As shown in Fig. 3b, the entire electrode had a clear deformation during the first cycling process. The electrode moved to the left side during the first 0.1 C lithiation and reached 4 µm movement. At the end of the second 0.05 C lithiation, the electrode moved an additional 5 µm to the left. Before the delithiation process, the 9 µm movement was calibrated so that all the particles have their original positions.

The electrode moved to the opposite direction during delithiation and 4 µm movement was achieved at the end of delithiation. It was noticed that the first 4 µm movement might potentially due to the sample holder shift during motion. However, the movement during the second lithiation is larger within a shorter period of time which indicates that the movement is mainly due to the volume change of Sn particles while the sample holder shift during the data acquisition has minor influences.
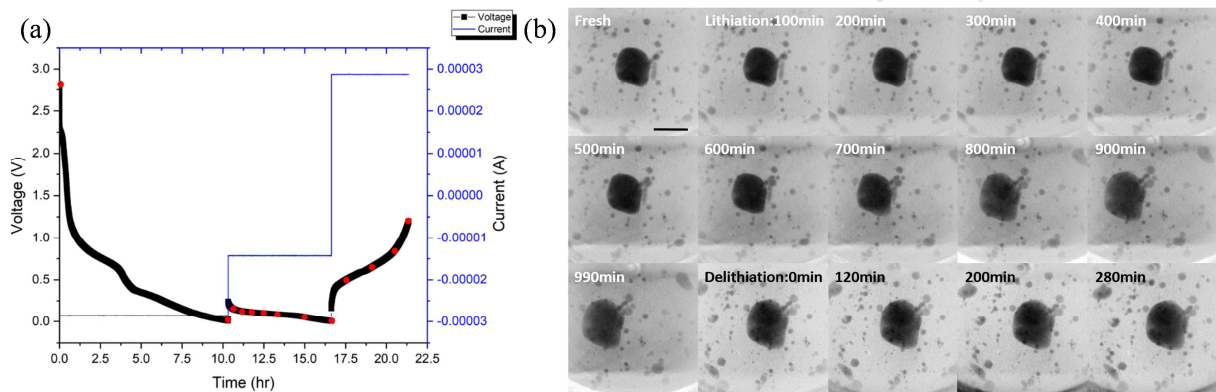

Fig. 3. (a) Voltage and current profiles of an in operando Sn cell. (b) TXM images at one of the ten positions during the first cycling process showing the movement of the electrode during lithiation and delithiation processes (as indicated in white during lithiation and black for delithiation) caused by electrode deformation and sample holder shift. The scale bar is 10 µm.

At the ten positions for imaging, several hundreds of particles with different sizes have been monitored by the in operando TXM. Less than 3% of the particles don't have any volume change during the first cycle. We believe that the main reason is the loss of electrical connection for those particles. Among the active particles, 4 particles at different positions with different sizes were selected to evaluate the effect of size on the dynamic morphological changes. In order to

eliminate the effect of shape, spherical particles were selected. The largest one is not spherical because there was no spherical one at this size. As shown in Fig. 4, the original sizes are 1 µm, 2 µm, 3.4 µm, and 10 µm in diameter or area equivalent diameter in pristine condition. The contours in these selected particles demonstrate the area change of the projection images during the first cycling process. The relative area which stands for the ratio between the current area to its original area was measured via contour analysis in ImageJ based on the intensity gradient of each specific image. The particles have relatively smooth contours and a 150% overall 2D area expansion (on average) was achieved at the end of the 0.05 C lithiation as shown in Fig. 5. At the end of the first delithiation, the particles shrink around 10% and they are not able to recover their original sizes. The reasons could be the formation of nanopores inside the particle [12, 24-26] during delithiation and the loss of electrical connection [19, 27, 28].
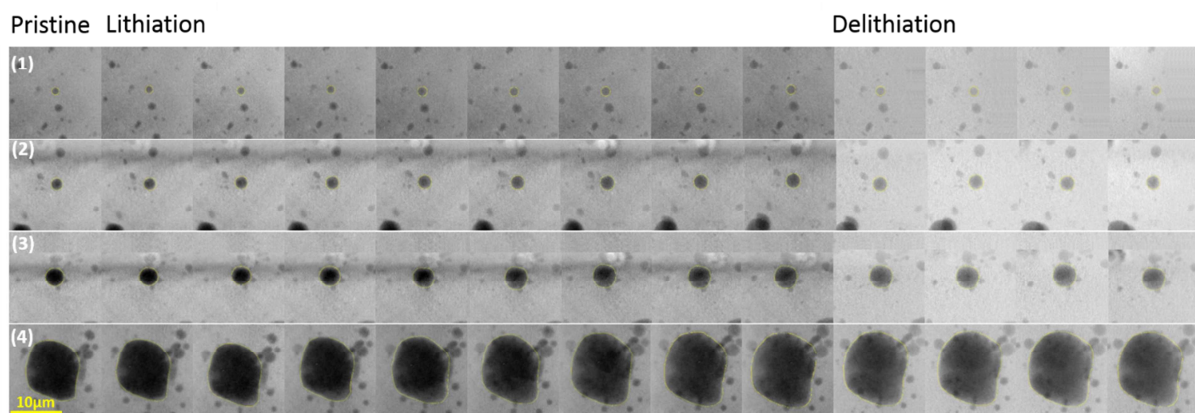
Fig. 4. Corresponding TXM images for the selected particles at the time steps highlighted in Fig. 3a.
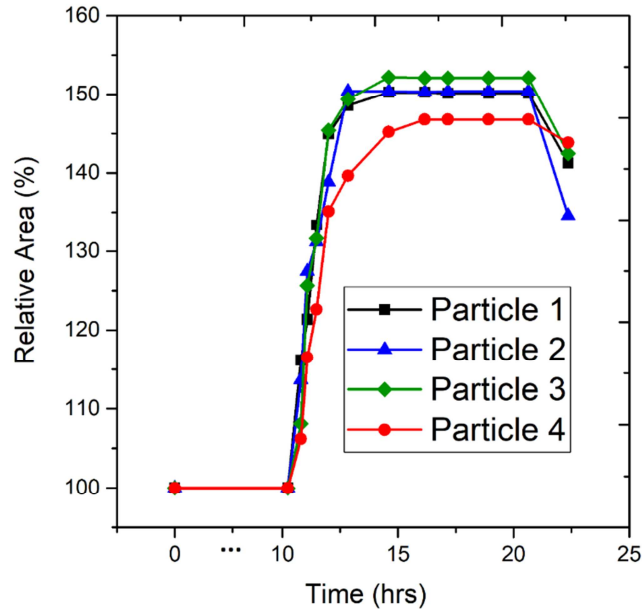
Fig. 5. Dynamic two-dimensional area evolution calculated from the projected TXM images for the selected particles.

It was observed that regardless of particle size, volume expansion occurred simultaneously which is different from the phenomenon observed by Chao et al. [24, 29]. They found that the smaller Sn particles expand in a much faster pace than the larger particles. The major difference between the two in operando experiments was the lithiation process after the first constant current lithiation. Chao et al. did not observe the volume change at the end of the first constant current lithiation. Then a constant voltage lithiation at 0.001 V was implemented. In our case, the second lithiation is still constant current. This phenomenon can be explained by the negative feedback mechanism proposed by Yan et al. [30]. As shown in Eq.1, lithium ion intercalation reaction across the interfaces of electrolyte and Sn particles can be determined by the Butler-Volmer equation:

12

$$J^{\text{Li}} = \frac{J}{F} = \frac{i_0}{F} \left\{ \exp\left(\frac{\alpha F}{RT} \eta \right) - \exp\left[-\frac{(1-\alpha)F}{RT} \eta \right] \right\} \qquad (1)$$

where J^{Li} and J are the reaction flux of lithium ion and reaction current density respectively, R is the universal gas constant, T is absolute temperature, F is Faraday's constant, i_0 is the exchange current density, η is the surface overpotential, and α is a symmetry factor that represents the fraction of the applied potential promoting the cathodic reaction, α is 0.5 for the electrochemical reaction in LIBs. The overpotential η is defined as below:

$$\eta = \emptyset_1 - \emptyset_2 - U_{OCP} \qquad (2)$$

Where $\emptyset_1$ and $\emptyset_2$ are the potential of Sn particles and electrolyte at the interface respectively, and U_{OCP} is the open circuit potential (OCP) at the interface. It should be noted that the overpotential is a negative value during lithiation and a positive value during delithiation.

If the battery is cycled at a low rate, such as 0.1 C and 0.05 C, we can assume that the exchange current density i_0 is constant at the Sn particle/electrolyte interface for all the particles in the electrode. Then the lithium ion intercalation rate on the surface of Sn particles is determined by the overpotential η. Due to the low rate cycling, high electronic conductivity of Sn, and high ionic conductivity of the electrolyte, we also can assume that both $\emptyset_1$ and $\emptyset_2$ have very small spatial variation in the electrode and the value of $\emptyset_1$ - $\emptyset_2$ is the same for all the Sn particles in the electrode. Therefore, the difference of lithium intercalation rate on the surface of different Sn particles in the electrode is only determined by the OCP. The OCP is determined by the lithium ion concentration on the surface of Sn particles. As shown in the literature [6, 22, 31-

33], the OCP of Sn decreases when the lithium concentration increases on the surface. During a constant current lithiation, the value of $\emptyset_1$ - $\emptyset_2$ also decreases to keep a certain overpotential for the constant current. If we assume that the lithium concentration on the surface of smaller Sn particles increases faster than it on the surface of larger particles at the beginning of lithiation process, the higher lithium concentration on the surface of smaller particles causes smaller OCP. According to Eq. 2, overpotential decreases when OCP decreases assuming all the Sn particles have the same $\emptyset_1$ - $\emptyset_2$, which leads to a lower intercalation rate. The lower intercalation rate slows down the lithium concentration increase on the surface. At certain lithium concentration level, $OCP = \emptyset_1$ - $\emptyset_2$ and the overpotential could be zero, which completely stops the intercalation reaction. This is a negative feedback mechanism caused by the interaction among heterogeneous particles in the electrode. However, if the battery cell is operated at constant voltage mode, the value of $\emptyset_1$ - $\emptyset_2$ almost does not change as the lithiation process proceeds. The interaction of particles doesn't exist, and all the particles react at their own paces. The smaller particles proceed faster due to their larger surface to volume ratio. However, the negative feedback mechanism could be invalid at high current rates. High current rate means fast electron and lithium ion transport, which can cause large polarization and large lithium ion concentration difference in the electrode. We cannot assume that i_0 (the exchange current density), $\emptyset_1$ and $\emptyset_2$ (the potential of Sn particles and electrolyte at the interface) have very small spatial variation in the electrode with large polarization and lithium ion concentration difference. According to Eqs. 1 and 2, the dynamic volume change of the particles is related to the local environment of the particle.
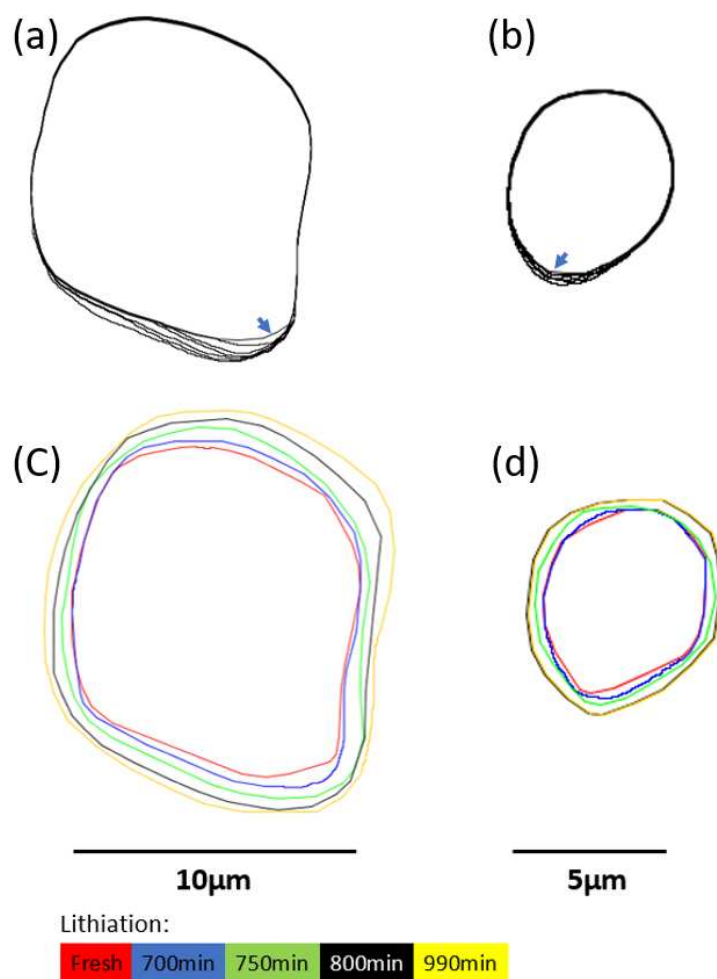
Fig. 6. Contour plots for two selected Sn particles (a,b) during the first 50 min of volume expansion and (c,d) at the specified time steps during the lithiation process. The arrows in a and b point to the expansion direction.

To investigate the effect of shape on the dynamic morphological change of Sn particles, the curvature related analysis was performed in Avizo® by registering all contour plots into the same coordinate via the combination of contour line and gravitational center. The contours from the 2D in operando images in Fig. 6a and b display the dynamic changes during the first 50 min when the volume expansion occurred. The increment between each time step was 10 min. The

arrows are pointing to the direction of volume expansion. It reveals that the volume expansion of irregular-shaped Sn particles is more likely to take place at the surface with higher curvature and more details can be found in the video in the supplemental document. We believe that this phenomenon was caused by a higher average bulk lithium concentration at the sharp locations. Volume change is mainly determined by the average bulk lithium concentration, not by the surface lithium concentration. The negative feedback mechanism is still valid in different regions of a single particle. The difference between the single particle case and the multiple particle case is the transport of lithium. Lithium can move inside a single particle but cannot move between particles during the lithiation or delithiation processes. Although the lithium concentration should have a small variation on the surface of a single particle, the region with higher curvature will have a larger average bulk lithium concentration, which cause earlier expansion, as shown in Fig. 6a and b. To further explain this phenomenon, we conducted a numerical simulation on lithium transport in a water drop-shaped particle using finite element method as shown in the supporting information. The radius of the small curvature end of the particle is 5 µm (0.2 µm^{-1} curvature) and that of the large curvature end is 1 µm (1 µm^{-1} curvature). A fixed lithium ion concentration is imposed on the surface of the particle. The lithium ion diffuses from the surface to the center because of the concentration difference. As shown in Fig. S1b-d, the average bulk lithium ion concentration increases much faster in the large curvature end than it does in the small curvature end, which means that the large curvature end expands earlier. Fig. 6c and d displayed the contour line of the selected particles at five specific time steps during the lithiation process as indicated in the color bar. After the region with high curvature expanded, it was observed that the entire particle expanded thereafter.
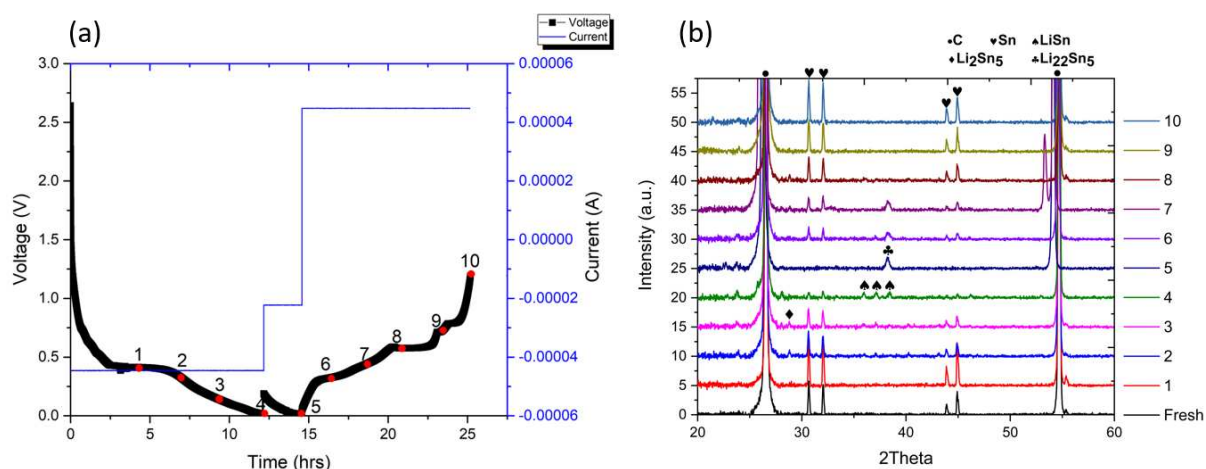
Fig. 7. (a) Voltage and current profiles of an ex situ Sn cell and (b) the corresponding XRD patterns at the time steps shown in (a).

An ex situ XRD experiment was performed to monitor the dynamic crystalline changes during the first cycle. The states of charge at which the XRD data were collected was depicted on the voltage profile shown in Fig. 7a. In this XRD experiment, we applied 0.1 C and 0.05 C for lithiation and 0.1 C for delithiation during the first cycle to duplicate the same situation as the in operando TXM experiment. As shown in Fig. 7b, we observed that the lithiation and delithiation processes of Sn particles complied the following sequence:

$$Sn \rightarrow Li_2Sn_5 \rightarrow LiSn \rightarrow Li_{22}Sn_5 \rightarrow LiSn \rightarrow Sn \qquad (3)$$
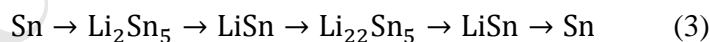
When the cell voltage reaches the first plateau at 0.56 V, the Sn phase starts to vanish and a crystalline Li_2Sn_5 phase is formed. LiSn was observed at the end of the 0.1 C lithiation, but $Li_{22}Sn_5$ phase was not observed. Since LiSn phase (51%) has a relatively smaller volume expansion than $Li_{22}Sn_5$ phase (260%), this result verifies why the in operando TXM experiment

17

did not show clear morphological change after the first 0.1 C lithiation. During the second 0.05 C lithiation, the Sn particles were lithiated to $Li_{22}Sn_5$ phase. During the 0.1 C delithiation process, the XRD results show that $Li_{22}Sn_5$ phase disappears and Sn phase reappears at the end of delithiation. This ex situ XRD results are in accord with the in situ synchrotron XRD data of the Sn electrode acquired during the first lithiation-delithiation cycle shown in Ref [24]. As shown in Fig. 5, most of the Sn particles did not recover their original size after delithiation, which is not in accord with the ex situ XRD results. The reasons could be the formation of nanometer-sized pores during delithiation [12, 24-26] and the loss of electrical connection [19, 27, 28].

4. Conclusion

In this work, the dynamic morphological evolution of Sn particles during lithiation and delithiation processes was investigated using an in operando synchrotron TXM imaging technique. The relative area analysis based on the in operando 2D TXM images demonstrates that all the active Sn particles expanded simultaneously with almost the same pace regardless particle size if the battery cell is operated at constant current mode. This phenomenon is due to a negative feedback mechanism in a heterogeneous battery electrode. If the particle shape is not spherical, the contour analysis results show that the regions with higher curvature in a single particle start volume expansion first at the very beginning of the volume change process. After that, the entire particle expanded almost homogeneously.

References:

[1] T.M. Bandhauer, S. Garimella, T.F. Fuller, A Critical Review of Thermal Issues in Lithium-Ion Batteries, Journal of the Electrochemical Society, 158 (2011) R1-R25.

[2] H.X. Kang, C. Lim, T.Y. Li, Y.Z. Fu, B. Yan, N. Houston, V. De Andrade, F. De Carlo, L.K. Zhu, Geometric and Electrochemical Characteristics of LiNi1/3Mn1/3Co1/3O2 Electrode with Different Calendering Conditions, Electrochimica Acta, 232 (2017) 431-438.

[3] C. Lim, B. Yan, H.X. Kang, Z.B. Song, W.C. Lee, V. De Andrade, F. De Carlo, L.L. Yin, Y. Kim, L.K. Zhu, Analysis of geometric and electrochemical characteristics of lithium cobalt oxide electrode with different packing densities, Journal of Power Sources, 328 (2016) 46-55.

[4] B. Yan, C.W. Lim, Z.B. Song, L.K. Zhu, Analysis of Polarization in Realistic Li Ion Battery Electrode Microstructure Using Numerical Simulation, Electrochimica Acta, 185 (2015) 125-141.

[5] T.A.O. Zheng, J.R. Dahn, CHAPTER 11 - Applications of Carbon in Lithium-Ion Batteries A2 - Burchell, Timothy D, Carbon Materials for Advanced Technologies, Elsevier Science Ltd, Oxford, 1999, pp. 341-387.

[6] A.R. Kamali, D.J. Fray, TIN-BASED MATERIALS AS ADVANCED ANODE MATERIALS FOR LITHIUM ION BATTERIES: A REVIEW, Reviews on Advanced Materials Science, 27 (2011) 14-24.

[7] S. Goriparti, E. Miele, F. De Angelis, E. Di Fabrizio, R.P. Zaccaria, C. Capiglia, Review on recent progress of nanostructured anode materials for Li-ion batteries, J. Power Sources, 257 (2014) 421-443.

[8] G. Ehrlich, C. Durand, X. Chen, T. Hugener, F. Spiess, S. Suib, Metallic negative electrode materials for rechargeable nonaqueous batteries, J. Electrochem. Soc., 147 (2000) 886-891.

[9] L. Beaulieu, K. Eberman, R. Turner, L. Krause, J. Dahn, Colossal reversible volume changes in lithium alloys, Electrochem. Solid-State Lett., 4 (2001) A137-A140.

[10] M. Zhang, T. Wang, G. Cao, Promises and challenges of tin-based compounds as anode materials for lithium-ion batteries, Int. Mater. Rev., 60 (2015) 330-352.

[11] H.X. Dang, K.C. Klavetter, M.L. Meyerson, A. Heller, C.B. Mullins, Tin microparticles for a lithium ion battery anode with enhanced cycling stability and efficiency derived from Se-doping, J. Mater. Chem. A, 3 (2015) 13500-13506.

[12] X. Zhou, T. Li, Y. Cui, Y. Fu, Y. Liu, L. Zhu, In Situ Focused Ion Beam Scanning Electron Microscope Study of Microstructural Evolution of Single Tin Particle Anode for Li-Ion Batteries, ACS Applied Materials & Interfaces, 11 (2019) 1733-1738.

[13] Y. Cui, T.Y. Li, X.W. Zhou, A. Mosey, W. Guo, R.H. Cheng, Y.Z. Fu, L.K. Zhu, Electrochemical behavior of tin foil anode in half cell and full cell with sulfur cathode, Electrochimica Acta, 294 (2019) 60-67.

[14] C.K. Chan, H. Peng, G. Liu, K. McIlwrath, X.F. Zhang, R.A. Huggins, Y. Cui, High-performance lithium battery anodes using silicon nanowires, Nature Nanotechnology, 3 (2008) 31-35.

[15] T. Kennedy, E. Mullane, H. Geaney, M. Osiak, C. O'Dwyer, K.M. Ryan, High-Performance Germanium Nanowire-Based Lithium-Ion Battery Anodes Extending over 1000 Cycles Through in Situ Formation of a Continuous Porous Network, Nano Letters, 14 (2014) 716-723.

[16] X.H. Liu, S. Huang, S.T. Picraux, J. Li, T. Zhu, J.Y. Huang, Reversible Nanopore Formation in Ge Nanowires during Lithiation-Delithiation Cycling: An In Situ Transmission Electron Microscopy Study, Nano Letters, 11 (2011) 3991-3997.

[17] J. Liu, Y. Li, X. Huang, R. Ding, Y. Hu, J. Jiang, L. Liao, Direct growth of SnO2 nanorod array electrodes for lithium-ion batteries, Journal of Materials Chemistry, 19 (2009) 1859-1864.

[18] J.Y. Huang, L. Zhong, C.M. Wang, J.P. Sullivan, W. Xu, L.Q. Zhang, S.X. Mao, N.S. Hudak, X.H. Liu, A. Subramanian, H. Fan, L. Qi, A. Kushima, J. Li, In Situ Observation of the Electrochemical Lithiation of a Single SnO2 Nanowire Electrode, Science, 330 (2010) 1515-1520.

[19] H.X. Dang, K.C. Klavetter, M.L. Meyerson, A. Heller, C.B. Mullins, Tin microparticles for a lithium ion battery anode with enhanced cycling stability and efficiency derived from Se-doping, Journal of Materials Chemistry A, 3 (2015) 13500-13506.

[20] M. Ebner, F. Marone, M. Stampanoni, V. Wood, Visualization and Quantification of Electrochemical and Mechanical Degradation in Li Ion Batteries, Science, 342 (2013) 716.

[21] F. Sun, H. Markötter, D. Zhou, S.S.S. Alrwashdeh, A. Hilger, N. Kardjilov, I. Manke, J. Banhart, In Situ Radiographic Investigation of (De)Lithiation Mechanisms in a Tin-Electrode Lithium-Ion Battery, ChemSusChem, 9 (2016) 946-950.

[22] J. Wang, Y.-c.K. Chen-Wiegart, J. Wang, In Situ Three-Dimensional Synchrotron X-Ray Nanotomography of the (De)lithiation Processes in Tin Anodes, Angewandte Chemie International Edition, 53 (2014) 4460-4464.

[23] B.C.a.J.M.M. A. Buades, A non-local algorithm for image denoising, IEEE Computer Society Conference on Computer Vision and Pattern Recognition, 2 (2005).

[24] S.-C. Chao, Y.-F. Song, C.-C. Wang, H.-S. Sheu, H.-C. Wu, N.-L. Wu, Study on Microstructural Deformation of Working Sn and SnSb Anode Particles for Li-Ion Batteries by in Situ Transmission X-ray Microscopy, The Journal of Physical Chemistry C, 115 (2011) 22040-22047.

[25] Q.Q. Li, P. Wang, Q. Feng, M.M. Mao, J.B. Liu, S.X. Mao, H.T. Wang, In Situ TEM on the Reversibility of Nanosized Sn Anodes during the Electrochemical Reaction, Chemistry of Materials, 26 (2014) 4102-4108.

[26] J.W. Wang, F.F. Fan, Y. Liu, K.L. Jungjohann, S.W. Lee, S.X. Mao, X.H. Liu, T. Zhu, Structural Evolution and Pulverization of Tin Nanoparticles during Lithiation-Delithiation Cycling, Journal of the Electrochemical Society, 161 (2014) F3019-F3024.

[27] M. Zhang, T. Wang, G. Cao, Promises and challenges of tin-based compounds as anode materials for lithium-ion batteries, International Materials Reviews, 60 (2015) 330-352.

[28] C. Lim, H.X. Kang, V. De Andrade, F. De Carlo, L.K. Zhu, Hard X-ray-induced damage on carbon-binder matrix for in situ synchrotron transmission X-ray microscopy tomography of Li-ion batteries, Journal of Synchrotron Radiation, 24 (2017) 695-698.

[29] S.C. Chao, Y.C. Yen, Y.F. Song, Y.M. Chen, H.C. Wu, N.L. Wu, A study on the interior microstructures of working Sn particle electrode of Li-ion batteries by in situ X-ray transmission microscopy, Electrochemistry Communications, 12 (2010) 234-237.

[30] B. Yan, C. Lim, L. Yin, L. Zhu, Three Dimensional Simulation of Galvanostatic Discharge of LiCoO2 Cathode Based on X-ray Nano-CT Images, Journal of the Electrochemical Society, 159 (2012) A1604-A1614.

[31] M. Winter, J.O. Besenhard, Electrochemical lithiation of tin and tin-based intermetallics and composites, Electrochimica Acta, 45 (1999) 31-50.

[32] J. Yang, Y. Takeda, N. Imanishi, O. Yamamoto, Ultrafine Sn and SnSb0.14 powders for lithium storage matrices in lithium-ion batteries, Journal of the Electrochemical Society, 146 (1999) 4009-4013.

[33] L. Bazin, S. Mitra, P.L. Taberna, P. Poizot, M. Gressier, M.J. Menu, A. Barnabe, P. Simon, J.M. Tarascon, High rate capability pure Sn-based nano-architectured electrode assembly for rechargeable lithium batteries, Journal of Power Sources, 188 (2009) 578-582.